JSTT JOURNAL OF SCIENCE AND TRANSPORT TECHNOLOGY

Journal of Science and Transport Technology
Journal homepage: https://jstt.vn/index.php/en

UNIVERSITY OF TRANSPORT TECHNOLOGY

Reduced isogeometric model for vibration analysis of beams under damping based on a fifth-order generalized shear deformation theory

Tan T. Nguyen[1,2], Quan M. Lieu[1,2], Ngoc Son Be[3], Qui X. Lieu[1,2,*]
[1]Faculty of Civil Engineering, Ho Chi Minh City University of Technology (HCMUT), 268 Ly Thuong Kiet Street, Dien Hong Ward, Ho Chi Minh City 700000, Vietnam
[2]Vietnam National University Ho Chi Minh City (VNU-HCM), Linh Xuan Ward, Ho Chi Minh City 700000, Vietnam
[3]AMS4 Research Group (Advanced Materials and Smart Structure for Sustainable System), University of Transport Technology, 54 Trieu Khuc Street, Thanh Liet Ward, Hanoi, Vietnam

Article info
Type of article:
Original research paper

DOI:
https://doi.org/10.58845/jstt.utt.2026.en.6.4.88-107

[*]**Corresponding author:**
Email address:
lieuxuanqui@hcmut.edu.vn

Received: 22/02/2026
Received in Revised Form: 18/06/2026
Accepted: 27/06/2026

Abstract: This work aims to use the reduced isogeometric model for analyzing the vibration behavior of beams under damping based on a fifth-order generalized shear deformation theory (GSDT). This beam theory utilizes the fifth-order polynomial function to represent the displacements through the beam height. Whilst the isogeometric analysis (IGA) employs B-spline functions to approximate the displacements along the beam length. These basis functions can easily meet the requirement of high-order derivatives which come from the fifth-order shear deformation theory. In the reduced IGA, instead of establishing the finite element model with all degrees of freedom (DOFs), only a given number of DOFs are kept to derive the algebraic equation systems condensed in state space for damping vibration analysis. The vibration responses of beams with different boundary conditions, length-to-height ratios and damping intensities are studied. The reliability and the accuracy of the reduced-order IGA are verified by comparing the damping-free results with other existing publications. Meanwhile, the corresponding outcomes considering damping are reported and discussed in detail. Such solutions can be referred to by future research.

Keywords: Damped vibration; Beams; State space; Isogeometric analysis; Fifth-order generalized shear deformation theory.

1. Introduction

Beams are fundamental structural components which are widely used in engineering systems such as civil buildings, bridges and industrial structures. With the extremely useful possibility of resisting bending, shear and load transmission, beam responses directly affect the strength, stiffness and overall performance of the whole structural system. Therefore, studying the mechanical behavior of beams is necessary, and this can help to clarify the relationship between loads, boundary conditions, material features as well as structural responses including displacements, stresses, strains, natural vibration frequencies, and so on. This reveals that those quantities are extremely important for designing and evaluating the structural safety. Thus, accurately simulating the mechanical responses of beams is essential from both theoretical and practical points of view.

In this regard, numerous beam theoretical models have been developed to analyze their mechanical behavior. Basically, the well-known Euler–Bernoulli theory [1] is one of the simplest and classical models which is only suitable for thin beams. In this model, the shear strain effect is ignored, and the cross-section still remains plane and perpendicular to the neutral axis after deformation. To overcome these limitations, the Timoshenko beam theory [2] which is known by another name as the first-order shear deformation theory (FSDT) is proposed. Although the shear influence is considered, the transverse shear strain is assumed to be constant through the beam thickness. Moreover, the shear-free stresses at the top and bottom surfaces exist. As a consequence, a shear correction coefficient is required to yield better results. It is clear that supplementing such a factor causes several shortcomings and limited applications of this theory to many problems, especially for thin-to-thick beams with composite materials. Nevertheless, the so-called shear locking phenomenon can be occured if shape functions used to interpolate the transverse displacement and rotation fields are incompatible.

Accordingly, high-order shear deformation theories (HSDTs) have been proposed to tackle the above-indicated issues. Since the displacements through the thickness are represented by higher - order polynomials [3, 4], exponential functions [5], or trigonometric and hyperbolic functions [6, 7], etc. Thus, the nonlinear transverse shear strains can be more accurately simulated without further adding shear correction coefficients. Additionally, the zero transverse shear stresses on the top and bottom surfaces are satisfied naturally.

Then, numerous variations of these HSDTs have also been developed that can be listed as refined and quasi-3D theories [8]. Although the success of these theories has been validated via a large number of publications, most of them are only devoted to the traditional finite element method (FEM).

As known, such HSDTs often require high-order continuity of the displacement field due to the appearance of second- or higher-order derivatives in their weak form. It is obvious that in the FEM, the shape functions such as Lagrange or Hermite cubic functions cannot result in high-order continuity as desired in HSDTs. Consequently, the FEM is inefficient for modelling beams based on such theories. Furthermore, the shear locking phenomenon can occur if several special techniques such as reduced integration [9], or assumed-strain formulations [10, 11], are not applied.

To overcome these shortcomings, the isogeometric analysis (IGA) [12] was proposed as an efficient numerical framework. This method utilizes the same B-spline or NURBS basis functions to precisely describe any complex geometries and approximately resolve the displacement, strain and stress fields. Owing to the salient properties of the above basis functions, especially in easily achieving high-order continuity and derivatives by selecting a proper degree, the IGA can yield competitive solutions, even with high accuracy in comparison with the FEM for the same mesh level in many problem kinds. For those reasons, this numerical approach has been broadly applied to a variety of fields [13–16].

It can be found that most current researches employing the IGA focus primarily on structural free vibrations without many thorough and full studies on the damping influence on their behavior [17–19]. Indeed, damping plays a crucial role in structural behavior analysis due to its energy dissipation. As a result, dynamic responses over time can be overestimated if it is ignored. This leads to an unreliable analysis of structural behavior, even an incorrect assessment of working conditions in the structural health monitoring (SHM) area.

Also concerning the SHM field, directly measuring the signals of a monitored structure with all DOFs is impractical, especially for large-scale structures. In addition, due to the limitations on the number of sensors, cost, and installation conditions, real-world data are often collected only at a finite number of DOFs. Then, the information on the remaining DOFs without sensors can be numerically inferred by ROM strategies [20, 21]. Thereby, the computational and measurement costs can be reduced dramatically. For such advantages, numerous MOR techniques have been studied [22]. Nonetheless, no ROM constructed by a combination of the IGA and a fifth-order GSDT for the vibration analysis of beams has been published up to this point. Consequently, this research is conducted herein as a novel contribution.

2. Basic theories

2.1. Fifth-order generalized shear deformation theory

Assume that a beam has an arbitrary section in the y-z plane and the length L in the $x-$axis. Its width and height are symbolized as b and h with regard to the $y-$ and $z-$axes, respectively. Accordingly, the displacements at an arbitrary point through the z-direction can be generally described by the following GSDT:

$$\begin{cases} u(x,z) = u_0(x) - z\dfrac{dw_0(x)}{dx} + \chi(z)\theta_0(x) \\ w(x,z) = w_0(x), \quad -\dfrac{h}{2} \le z \le +\dfrac{h}{2} \end{cases} \tag{1}$$

where u_0 and w_0 denote the straight displacements given at the neutral axis $(z=0)$ in the $x-$ and $z-$directions, respectively; $\theta_0(x)$ stands for the slope about the *y*-axis caused by the bending behavior.

And finally, $\chi(z)$ symbolizes the high-order polynomial function used to represent the displacement, strain and stress fields through the beam height. This function is derived based on the following criterion: (i) an odd function of the thickness corrdinate about the mid-plane to ensure physical consistency and decoupling between bending and shear, i.e. $\chi(-z) = -\chi(z)$; (ii) no transverse shear stresses at the top and bottom surface to naturally satisfy boundary conditions, i.e. $\tau_{xz}\left(z = \pm\dfrac{h}{2}\right) = 0$; (iii) $\chi(z=0) = 0$ to result in no membrane strain and normal stress, but give a maximum shear stress at $z=0$; (iv) $\chi(z)$ must be smoothness and differentiability to demand the stress-strain relationship, and (v) no shear correction factor, but still give a high compatibility with 3D solutions.

For the above rules, according to Ref. [23], $\chi(z)$ is given as follows

$$\chi(z) = \frac{\pi}{h}z - \frac{9\pi}{5h^3}z^3 + \frac{28\pi}{25h^5}z^5 \tag{2}$$

According to Ref. [23], this fifth-order polynomial function is sufficient to more accurately represent the strain and stress fields through the height of thick plates with composite materials, especially under the size effects caused by the nonlocal elasticity theory. This function has also been applied in several publications to analyze the mechanical behavior of plate structures [24, 25]. Nonetheless, using the above plate theories to model other structural members such as beams, columns, etc. is not completely suitable in most cases in practice, especially for the compatibility of geometric dimensions and strain fields when modeling beams with plates. In such cases, the plate model always requires a significantly larger number of DOFs since more dimensions are considered for formulation. Accordingly, its computational cost is remarkably increased without a more effective improvement in accuracy. Moreover, the plate model does not appropriately reflect the one-dimensional deformation mechanism of beams. It is clear that reports on such beams have been relatively limited so far. Hence, it is adopted to study the vibration behavior of beam structures in this work.

Now, the axial and transverse shear strains can be computed as follows

$$\varepsilon_{xx} = \frac{\partial u(x,z)}{\partial x} = \frac{\partial u_0}{\partial x} - z\frac{d^2 w_0}{dx^2} + \chi\frac{\partial \theta_0}{\partial x} \quad (3)$$

$$\gamma_{xz} = \frac{\partial u(x,z)}{\partial z} + \frac{\partial w(x,z)}{\partial x} = \frac{d\chi}{dz}\theta_0 \quad (4)$$

In the case of the homogeneous beam, the corresponding stresses can be calculated as follows

$$\sigma_{xx} = E\varepsilon_{xx} \quad (5)$$

$$\tau_{xz} = G\gamma_{xz} = \frac{E}{2(1+\nu)}\gamma_{xz} \quad (6)$$

where E and G denote the Young's modulus and shear modulus, respectively, and ν stands for Poisson's ratio.

Relating to σ_{xx}, the internal forces include

$$N = \int_{-\frac{h}{2}}^{+\frac{h}{2}} \sigma_{xx} dz \quad (7)$$

$$M = \int_{-\frac{h}{2}}^{+\frac{h}{2}} z\sigma_{xx} dz \quad (8)$$

$$M_\chi = \int_{-\frac{h}{2}}^{+\frac{h}{2}} \chi\sigma_{xx} dz \quad (9)$$

In addition, the internal force regarding τ_{xz} is

$$Q = \int_{-\frac{h}{2}}^{+\frac{h}{2}} \tau_{xz} dz \quad (10)$$

Substituting ε_{xx} in Eq. (3) into σ_{xx} in Eq. (5), and γ_{xz} in Eq. (4) into τ_{xz} in Eq. (6), then, Eqs. (7), (8), (9) and (10) are rewritten as follows

$$N = \int_{-\frac{h}{2}}^{+\frac{h}{2}} E\left(\frac{\partial u_0}{\partial x} - z\frac{d^2 w_0}{dx^2} + \chi\frac{\partial \theta_0}{\partial x}\right) dz \quad (11)$$

$$M = \int_{-\frac{h}{2}}^{+\frac{h}{2}} zE\left(\frac{\partial u_0}{\partial x} - z\frac{d^2 w_0}{dx^2} + \chi\frac{\partial \theta_0}{\partial x}\right) dz \quad (12)$$

$$M_\chi = \int_{-\frac{h}{2}}^{+\frac{h}{2}} \chi E\left(\frac{\partial u_0}{\partial x} - z\frac{d^2 w_0}{dx^2} + \chi\frac{\partial \theta_0}{\partial x}\right) dz \quad (13)$$

$$Q = \int_{-\frac{h}{2}}^{+\frac{h}{2}} G\frac{d\chi}{dz}\theta_0 dz \quad (14)$$

For a more concise presentation, Eqs. (11), (12), (13) and (14) can be reexpressed as follows

$$\begin{Bmatrix} N \\ M \\ M_\chi \end{Bmatrix} = \int_{-\frac{h}{2}}^{+\frac{h}{2}} \begin{bmatrix} E & zE & E\chi \\ zE & z^2E & zE\chi \\ E\chi & zE\chi & E\chi^2 \end{bmatrix} \begin{Bmatrix} \frac{\partial u_0}{\partial x} \\ -\frac{d^2 w_0}{dx^2} \\ \frac{\partial \theta_0}{\partial x} \end{Bmatrix} dz \quad (15)$$

and

$$Q = \int_{-\frac{h}{2}}^{+\frac{h}{2}} G\frac{d\chi}{dz}\theta_0 dz \quad (16)$$

Now, following the Hamilton's principle, one has

$$\delta\int_{t_1}^{t_2} \left(W_I - W_E - E_K - W_D\right) dt = 0 \quad (17)$$

where $W_I = \frac{1}{2}\int_V \left(\sigma_{xx}\varepsilon_{xx} + \tau_{xz}\gamma_{xz}\right) dV$ denotes the internal work per the element volume V, and its variation is computed as

$$\begin{aligned} \delta W_I &= \int_V \left(\delta\varepsilon_{xx} E\varepsilon_{xx} + \delta\gamma_{xz} G\gamma_{xz}\right) dV \\ &= b\int_0^L \left[(\delta\boldsymbol{\kappa})^T \mathbf{C}_{mb}\boldsymbol{\kappa} + \delta\theta_0 C_s \theta_0\right] dx \end{aligned} \quad (18)$$

where

$$\boldsymbol{\kappa} = \begin{Bmatrix} \frac{\partial u_0}{\partial x} & -\frac{d^2 w_0}{dx^2} & \frac{\partial \theta_0}{\partial x} \end{Bmatrix}^T$$

and (19)

$$\delta\boldsymbol{\kappa} = \begin{Bmatrix} \frac{\partial \delta u_0}{\partial x} & -\frac{d^2 \delta w_0}{dx^2} & \frac{\partial \delta\theta_0}{\partial x} \end{Bmatrix}^T$$

$$\mathbf{C}_{mb} = \begin{bmatrix} c_0 & c_z & c_\chi \\ c_z & c_{z^2} & c_{z\chi} \\ c_\chi & c_{z\chi} & c_{\chi^2} \end{bmatrix} \quad (20)$$

$$C_s = \int_{-\frac{h}{2}}^{+\frac{h}{2}} G\left(\frac{d\chi}{dz}\right)^2 dz \quad (21)$$

in which

$$c_0, c_z, c_{z^2}, c_\chi, c_{z\chi}, c_{\chi^2} = \int_{-\frac{h}{2}}^{+\frac{h}{2}} E\left(1, z, z^2, \chi, z\chi, \chi^2\right) dz \quad (22)$$

Also in Eq. (17), $W_E = 0$ is the external work for the loading-free case. Moreover, $E_K = \frac{1}{2}\int_V \rho\left(\dot{u}^2 + \dot{w}^2\right) dV$ denotes the strain energy, and its variation is given as

$$\delta E_K = \int_V \rho\left(\delta\dot{u}\dot{u} + \delta\dot{w}\dot{w}\right)dV = b\int_0^L \left[\left(\delta\dot{\boldsymbol{\eta}}\right)^T \mathbf{m}_0\dot{\boldsymbol{\eta}} + i_0\delta\dot{w}_0\dot{w}_0\right]dx \tag{23}$$

in which the single dot represents the first derivative with regard to time t, and

$$\mathbf{m}_0 = \begin{bmatrix} i_0 & i_z & i_\chi \\ i_z & i_{z^2} & i_{z\chi} \\ i_\chi & i_{z\chi} & i_{\chi^2} \end{bmatrix} \tag{24}$$

$$i_0, i_z, i_{z^2}, i_\chi, i_{z\chi}, i_{\chi^2} = \int_{-\frac{h}{2}}^{+\frac{h}{2}} \rho\left(1, z, z^2, \chi, z\chi, \chi^2\right)dz \tag{25}$$

$$\dot{\boldsymbol{\eta}} = \left\{\dot{u}_0 \quad -\frac{d\dot{w}_0}{dx} \quad \dot{\theta}_0\right\}^T$$
$$\text{and} \quad \delta\dot{\boldsymbol{\eta}} = \left\{\delta\dot{u}_0 \quad -\frac{d\delta\dot{w}_0}{dx} \quad \delta\dot{\theta}_0\right\}^T \tag{26}$$

By applying integration by parts in time to Eq. (23), we obtain

$$\delta E_K = -b\int_0^L \left[\left(\delta\boldsymbol{\eta}\right)^T \mathbf{m}_0\ddot{\boldsymbol{\eta}} + i_0\delta w_0\ddot{w}_0\right]dx \tag{27}$$

where the double dot indicates the second derivative with regard to time t.

Moreover, also in Eq. (17), the work and its variation caused by damping forces are respectively computed as follows:

$$W_D = b\int_0^L \mathbf{q}^T\mathbf{r}_D dx \tag{28}$$

$$\delta W_D = -b\int_0^L \left(\delta\mathbf{q}\right)^T \mathbf{C}_D\dot{\mathbf{q}}dx \tag{29}$$

where $\mathbf{r}_D = -\mathbf{C}_D\dot{\mathbf{q}}$ is the damping force based on the assumption of proportional viscous damping with velocity; $\mathbf{C}_D$ is the matrix including damping coefficients, and $\dot{\mathbf{q}}$ is the first derivative of $\mathbf{q} = \left\{u_0 \quad w_0 \quad \theta_0\right\}^T$ in time t.

Finally, substituting Eqs. (18), (27) and (29) into Eq. (17), we attain the following weak form.

$$\begin{aligned} &b\int_0^L \left[\left(\delta\boldsymbol{\eta}\right)^T \mathbf{m}_0\ddot{\boldsymbol{\eta}} + i_0\delta w_0\ddot{w}_0\right]dx \\ &+b\int_0^L \left(\delta\mathbf{q}\right)^T \mathbf{C}_D\dot{\mathbf{q}}dx \\ &+b\int_0^L \left[\left(\delta\boldsymbol{\kappa}\right)^T \mathbf{C}_{mb}\boldsymbol{\kappa} + \delta\theta_0 C_s\theta_0\right]dx = 0 \end{aligned} \tag{30}$$

2.2. Full isogeometric model for damped vibration analysis

According to the IGA, the displacements of the eth NURB element are approximated by

$$\mathbf{q}_e = \sum_{i=1}^{nC} B_i\mathbf{q}_i \tag{31}$$

where B_i is the ith B-spline function [26]; $\mathbf{q}_i = \left\{u_{0,i} \quad w_{0,i} \quad \theta_{0,i}\right\}^T$ is the vector including DOFs at the ith control point, and nC is the number of control points in association with the eth element.

Substituting Eq. (31) into Eq. (30), we obtain

$$\mathbf{M}_e\ddot{\mathbf{q}}_e + \mathbf{C}_e\dot{\mathbf{q}}_e + \mathbf{K}_e\mathbf{q}_e = \mathbf{0} \tag{32}$$

where $\mathbf{M}_e$ and $\mathbf{K}_e$ denote the mass and stiffness matrices of the eth element. They are respectively calculated as follows:

$$\mathbf{M}_e = b\int_0^L \left[\left(\boldsymbol{\Lambda}_1\right)^T \mathbf{m}_0\boldsymbol{\Lambda}_1 + \left(\boldsymbol{\Lambda}_2\right)^T i_0\boldsymbol{\Lambda}_2\right]dx \tag{33}$$

$$\mathbf{K}_e = b\int_0^L \left[\left(\boldsymbol{\Theta}_{mb}\right)^T \mathbf{C}_{mb}\boldsymbol{\Theta}_{mb} + \left(\boldsymbol{\Theta}_s\right)^T C_s\boldsymbol{\Theta}_s\right]dx \tag{34}$$

in which

$$\boldsymbol{\Lambda}_1 = \begin{bmatrix} B_i & 0 & 0 \\ 0 & -B_{i,x} & 0 \\ 0 & 0 & B_i \end{bmatrix}, \quad \boldsymbol{\Lambda}_2 = \left\{0 \quad B_i \quad 0\right\} \tag{35}$$

$$\boldsymbol{\Theta}_{mb} = \begin{bmatrix} B_{i,x} & 0 & 0 \\ 0 & -B_{i,xx} & 0 \\ 0 & 0 & B_{i,x} \end{bmatrix}, \quad \boldsymbol{\Theta}_s = \left\{0 \quad 0 \quad B_i\right\} \tag{36}$$

In this work, the damping matrix $\mathbf{C}_e$ is given by the Rayleigh damping [27], its expression is

$$\mathbf{C}_e = \vartheta_1\mathbf{M}_e + \vartheta_2\mathbf{K}_e \tag{37}$$

with

$$\vartheta_1 = \xi\frac{2\omega_1\omega_2}{\omega_1+\omega_2}, \vartheta_2 = \xi\frac{2}{\omega_1+\omega_2} \tag{38}$$

where ξ denotes the damping ratio; $\omega_1\left(\text{rad/s}\right)$ and $\omega_2\left(\text{rad/s}\right)$ stand for the first two circular frequencies obtained from the free vibration analysis.

Then, assembling all matrices of each element into the global system, we have:

$$\mathbf{M}\ddot{\mathbf{q}} + \mathbf{C}\dot{\mathbf{q}} + \mathbf{K}\mathbf{q} = \mathbf{0} \tag{39}$$

Assume that the solution $\mathbf{q}$ in Eq. (39) is exponential, i.e. $\mathbf{q} = \boldsymbol{\Psi}e^{\lambda t}$. Now, substituting it into Eq. (39), we obtain

$$\left(\mathbf{M}\lambda^2+\mathbf{C}\lambda+\mathbf{K}\right)\mathbf{\Psi}=\mathbf{0} \tag{40}$$

or $$\mathbf{\Omega}\tilde{\mathbf{\Psi}}=\lambda\tilde{\mathbf{\Psi}} \tag{41}$$

where

$$\mathbf{\Omega}=\begin{bmatrix}\mathbf{0} & \mathbf{I}\\ -\mathbf{M}^{-1}\mathbf{K} & -\mathbf{M}^{-1}\mathbf{C}\end{bmatrix},\quad \tilde{\mathbf{\Psi}}=\begin{Bmatrix}\mathbf{\Psi}\\ \lambda\mathbf{\Psi}\end{Bmatrix} \tag{42}$$

By resolving Eq. (41) as an eigen problem, we obtain an eigenvalue matrix involving 2n eigenvalues on its diagonal line (n denotes the total number of DOFs after excluding those at boundaries). In which, the jth eigenvalue is

$$\lambda_j=-\xi_j\omega_{ud,j}\pm i\omega_{d,j} \tag{43}$$

in which $\xi_j=-\dfrac{\mathrm{Re}\left(\lambda_j\right)}{\left|\lambda_j\right|}$ stands for the jth damping ratio; $\omega_{d,j}=\mathrm{Im}\left(\lambda_j\right)$ and $\omega_{ud,j}=\dfrac{\omega_{d,j}}{\sqrt{1-\left(\xi_j\right)^2}}$ are the jth damped and undamped frequencies, respectively.

Moreover, Eq. (41) also yields an eigenvector matrix $\tilde{\mathbf{\Psi}}$, where $\tilde{\mathbf{\Psi}}_j=\begin{Bmatrix}\mathbf{\Psi}_j\\ \lambda_j\mathbf{\Psi}_j\end{Bmatrix}$ consists of the jth eigenvector (mode shape) $\mathbf{\Psi}_j$.

2.3. Reduced-order isogeometric model for damped vibration analysis

In this section, the ROM technique condensed in state space [28] is applied to the IGA. Now, by setting:

$$\mathbf{X}=\begin{bmatrix}\mathbf{0} & \mathbf{K}\\ \mathbf{K} & \mathbf{C}\end{bmatrix},\mathbf{Y}=\begin{bmatrix}-\mathbf{K} & \mathbf{0}\\ \mathbf{0} & \mathbf{M}\end{bmatrix} \tag{44}$$

Then, Eq. (39) is rewritten as follows

$$\mathbf{X}\tilde{\mathbf{\Psi}}=\mathbf{Y}\tilde{\mathbf{\Psi}}\tilde{\mathbf{\Lambda}} \tag{45}$$

where $\tilde{\mathbf{\Psi}}$ and $\tilde{\mathbf{\Lambda}}$ are the eigenvector matrix and eigenvalue matrix, respectively. They have the following forms.

$$\tilde{\mathbf{\Psi}}=\begin{bmatrix}\mathbf{\Psi} & \hat{\mathbf{\Psi}}\\ \mathbf{\Psi}\mathbf{\Lambda} & \hat{\mathbf{\Psi}}\hat{\mathbf{\Lambda}}\end{bmatrix},\tilde{\mathbf{\Lambda}}=\begin{bmatrix}\mathbf{\Lambda} & \mathbf{0}\\ \mathbf{0} & \hat{\mathbf{\Lambda}}\end{bmatrix} \tag{46}$$

where the symbols $\hat{\mathbf{\Psi}}$ and $\hat{\mathbf{\Lambda}}$ imply their corresponding complex conjugations.

In the ROM, the master DOFs "m" are kept, while the slave ones "s" are removed. And we have: n=m+s. For this, Eq. (44) can be separated as follows

$$\begin{gathered}\begin{bmatrix}\mathbf{X}_{mm} & \mathbf{X}_{ms}\\ \mathbf{X}_{sm} & \mathbf{X}_{ss}\end{bmatrix}\begin{Bmatrix}\tilde{\mathbf{\Psi}}_{mm}\\ \tilde{\mathbf{\Psi}}_{sm}\end{Bmatrix}=\\ \begin{bmatrix}\mathbf{Y}_{mm} & \mathbf{Y}_{ms}\\ \mathbf{Y}_{sm} & \mathbf{Y}_{ss}\end{bmatrix}\begin{Bmatrix}\tilde{\mathbf{\Psi}}_{mm}\\ \tilde{\mathbf{\Psi}}_{sm}\end{Bmatrix}\tilde{\mathbf{\Lambda}}\end{gathered} \tag{47}$$

where

$$\begin{aligned}
&\mathbf{X}_{mm}=\begin{bmatrix}\mathbf{0} & \mathbf{K}_{mm}\\ \mathbf{K}_{mm} & \mathbf{C}_{mm}\end{bmatrix}\\
&\mathbf{X}_{ms}=\left(\mathbf{X}_{sm}\right)^T=\begin{bmatrix}\mathbf{0} & \mathbf{K}_{ms}\\ \mathbf{K}_{ms} & \mathbf{C}_{ms}\end{bmatrix}\\
&\mathbf{X}_{ss}=\begin{bmatrix}\mathbf{0} & \mathbf{K}_{ss}\\ \mathbf{K}_{ss} & \mathbf{C}_{ss}\end{bmatrix}\\
&\mathbf{Y}_{mm}=\begin{bmatrix}-\mathbf{K}_{mm} & \mathbf{0}\\ \mathbf{0} & \mathbf{M}_{mm}\end{bmatrix}\\
&\mathbf{Y}_{ms}=\left(\mathbf{Y}_{sm}\right)^T=\begin{bmatrix}-\mathbf{K}_{ms} & \mathbf{0}\\ \mathbf{0} & \mathbf{M}_{ms}\end{bmatrix}\\
&\mathbf{Y}_{ss}=\begin{bmatrix}-\mathbf{K}_{ss} & \mathbf{0}\\ \mathbf{0} & \mathbf{M}_{ss}\end{bmatrix}
\end{aligned} \tag{48}$$

Because the purpose of the ROM is to eliminate DOFs "s" in Eq. (47), we set

$$\tilde{\mathbf{\Psi}}_{sm}=\mathbf{Z}\tilde{\mathbf{\Psi}}_{mm} \tag{49}$$

where the transform matrix $\mathbf{Z}$ is computed at the (k)th iteration as follows

$$\begin{gathered}\mathbf{Z}^{(k)}=\\ \mathbf{X}_{ss}^{-1}\left[\left(\mathbf{Y}_{sm}+\mathbf{Y}_{ss}\mathbf{Z}^{(k-1)}\right)\tilde{\mathbf{\Psi}}_{mm}\tilde{\mathbf{\Lambda}}_{mm}\tilde{\mathbf{\Psi}}_{mm}^{-1}-\mathbf{X}_{sm}\right]\end{gathered} \tag{50}$$

in which $\tilde{\mathbf{\Psi}}_{mm}$ and $\tilde{\mathbf{\Lambda}}_{mm}$ are obtained from

$$\mathbf{X}_Z\tilde{\mathbf{\Psi}}_{mm}=\mathbf{Y}_Z\tilde{\mathbf{\Psi}}_{mm}\tilde{\mathbf{\Lambda}}_{mm} \tag{51}$$

where

$$\begin{aligned}
&\mathbf{X}_Z=\mathbf{X}_{mm}+\mathbf{Z}^T\mathbf{X}_{sm}+\mathbf{X}_{ms}\mathbf{Z}+\mathbf{Z}^T\mathbf{X}_{ss}\mathbf{Z}\\
&\mathbf{Y}_Z=\mathbf{Y}_{mm}+\mathbf{Z}^T\mathbf{Y}_{sm}+\mathbf{Y}_{ms}\mathbf{Z}+\mathbf{Z}^T\mathbf{Y}_{ss}\mathbf{Z}
\end{aligned} \tag{52}$$

3. Results and discussion

In this section, a beam which is made of the ceramic material is studied. This ceramic material has the density $\rho=3960$ kg/m^3, Poisson's ratio $\nu=0.3$ and Young's modulus $E=380$ GPa. The free vibration behavior of this beam without damping was previously studied by using various HSDTs [6–8]. More concretely, Thai and Vo [6] investigated many variations of HSDTs, where a typical theory based on a third-order polynomial suggested by Reddy [29] was also studied. Nguyen et al. [7] suggested a HSDT based on a combination of inverse trigonometric and polynomial terms. Meanwhile, Vo et al. [8] introduced a quasi-3D theory constructed by a third-order polynomial [29]. In this work, for comparison with the existing publications, the nondimensional natural frequencies with and without damping are defined as follows:

$$\bar{\omega}_{ud/d,j} = \bar{\omega}_{ud/d,j}\frac{L^2}{h}\sqrt{\frac{\rho_{metal}}{E_{metal}}} \tag{53}$$

where $E_{metal} = 70$ GPa and $\rho_{metal} = 2702$ kg/m^3.

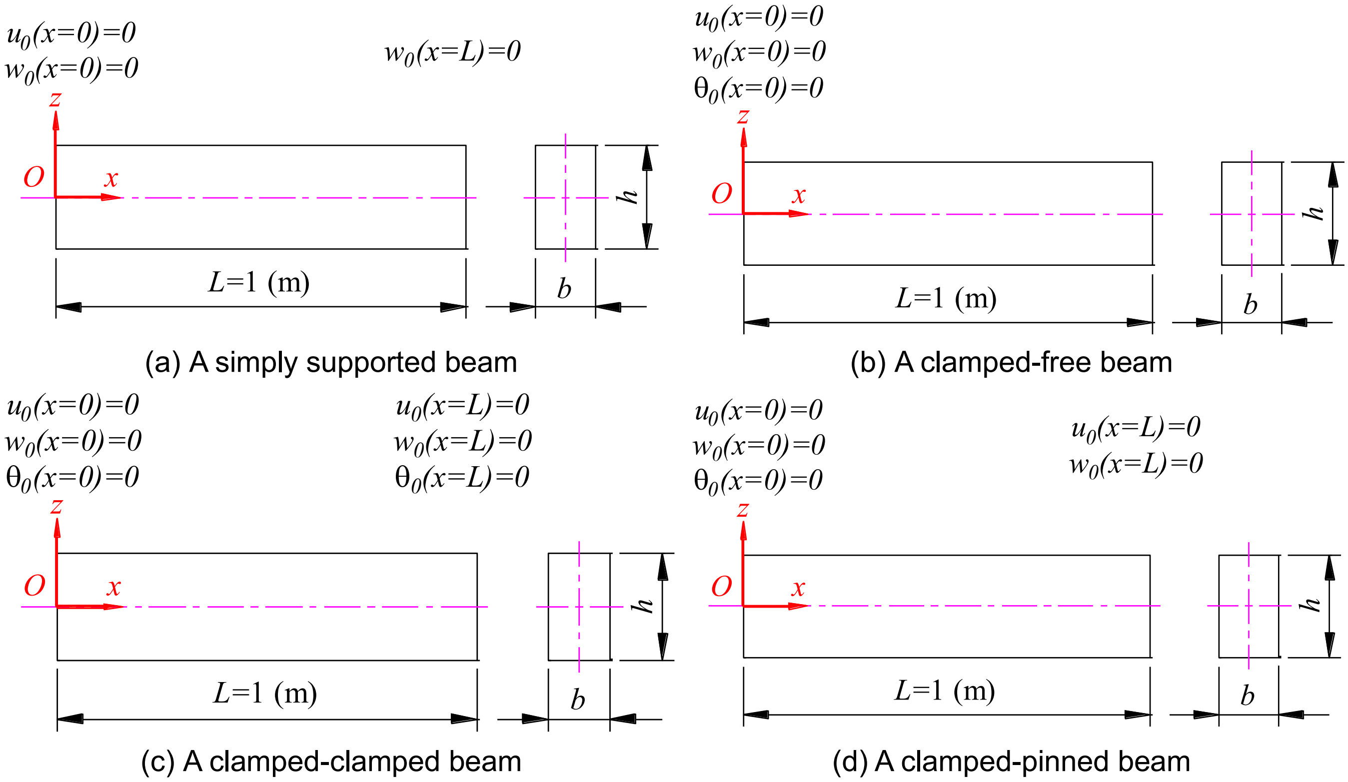

(a) A simply supported beam (b) A clamped-free beam

(c) A clamped-clamped beam (d) A clamped-pinned beam

Fig. 1. Schematic diagrams of four analyzed beams

Moreover, for a concise presentation, let us denote "C" as a clamped boundary $(u_0, w_0, \theta_0 = 0)$, "F" as a free one $(u_0, w_0, \theta_0 \neq 0)$, "S" as a roller $(w_0 = 0)$, and "P" as a pinned boundary $(u_0, w_0 = 0)$. For more specific visualization, schematic diagrams of four analyzed beams including the geometric configuration, coordinate system, and boundary conditions are plotted in Fig. 1.

3.1. Simply supported (P-S) beam

Firstly, the simply supported beam which is symbolized as P-S is investigated. In which, the boundary conditions at its two ends are pinned and roller, i.e. $u_0(0) = w_0(0) = w_0(L) = 0$.

Firstly, the full IGA based on the fifth-order GSDT is utilized for vibration analysis with $\xi = 5\,\%$ and two different length-to-span ratios, i.e. $\frac{L}{h} = 5$ and $\frac{L}{h} = 20$. Results obtained by different studies are reported in Table 1 for comparison. It can be seen that this beam only needs 17 cubic elements to achieve a good convergence with high accuracy compared with other reference solutions. Therefore, this mesh size is adopted for the subsequent examinations employing the reduced-order IGA.

Next, three different values of the damping ratio including $\xi = 3\,\%$, $\xi = 5\,\%$ and $7\,\%$ are investigated. Both the vertical and rotational DOFs at the control points numbered by 5, 7, 9, 11, 13 and 15 as plotted in Fig. 2 are selected to build the ROM. These control points are shown in red, while the others are in blue. The coordinates of all control points in the above figure are automatically defined from the computer-aided-design (CAD) environment [12]. Choosing the DOFs at such control points has a significant influence on the accuracy of a ROM. In this work, they are very carefully selected after examinations. The damped and undamped frequencies attained by the present method are summarized in Table 2. It is clear that the undamped frequencies match well with those of the above reference solutions. Moreover, the damped frequencies are always smaller than the undamped ones for the same mode. The larger the damping ratio is, the smaller the damped frequencies are, especially for higher-order modes. This reveals that the damping impact is remarkable that needs to be taken into account in the structural vibration analysis.

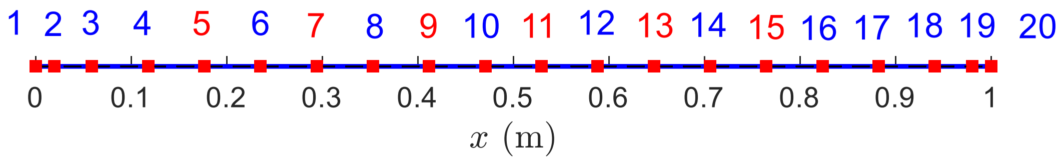

Fig. 2. Control points of 17 cubic elements

Table 1. The frequencies obtained by the full IGA and other references for the P-S beam with $\xi = 5\,\%$

$\frac{L}{h}$	Study	Mesh	Mode 1	2	3	4	5	6
5	$\bar{\omega}_{ud,j}$ [6]		5.1527	17.8812	34.2097	-	-	-
	$\bar{\omega}_{ud,j}$ [7]		5.1528	17.8817	34.2143	-	-	-
	$\bar{\omega}_{ud,j}$ [8]		5.1618	-	-	-	-	-
	Full IGA							
	$\bar{\omega}_{ud,j}$	11x11	5.1553	15.1157	17.9127	34.3497	45.3470	52.5239
	$\bar{\omega}_{d,j}$		5.1488	15.0968	17.8856	34.2093	45.0404	52.0557
	$\bar{\omega}_{ud,j}$	13x13	5.1552	15.1157	17.9117	34.3345	45.3470	52.4025
	$\bar{\omega}_{d,j}$		5.1488	15.0968	17.8846	34.1943	45.0404	51.9375
	$\bar{\omega}_{ud,j}$	15x15	5.1552	15.1157	17.9112	34.3279	45.3470	52.3522
	$\bar{\omega}_{d,j}$		5.1488	15.0968	17.8842	34.1878	45.0404	51.8885
	$\bar{\omega}_{ud,j}$	17x17	5.1552	15.1157	17.9110	34.3247	45.3470	52.3284
	$\bar{\omega}_{d,j}$		5.1488	15.0968	17.8840	34.1846	45.0404	51.8653
	$\bar{\omega}_{ud,j}$	19x19	5.1552	15.1157	17.9109	34.3230	45.3470	52.3159
	$\bar{\omega}_{d,j}$		5.1488	15.0968	17.8838	34.1829	45.0404	51.8531
20	$\bar{\omega}_{ud,j}$ [6]		5.4603	21.5732	47.5930	-	-	-
	$\bar{\omega}_{ud,j}$ [7]		5.4603	21.5732	47.5999	-	-	-
	$\bar{\omega}_{ud,j}$ [8]		5.4610	-	-	-	-	-
	Full IGA							
	$\bar{\omega}_{ud,j}$	11x11	5.4604	21.5763	47.6214	60.4627	82.6053	125.5887
	$\bar{\omega}_{d,j}$		5.4536	21.5493	47.4166	60.0586	81.6018	122.1022
	$\bar{\omega}_{ud,j}$	13x13	5.4604	21.5754	47.6102	60.4627	82.5312	125.2401
	$\bar{\omega}_{d,j}$		5.4536	21.5484	47.4056	60.0586	81.5302	121.7823
	$\bar{\omega}_{ud,j}$	15x15	5.4604	21.5750	47.6054	60.4627	82.4999	125.0986

Table 1. (continued)

$\frac{L}{h}$	Study	Mesh	Mode 1	2	3	4	5	6
	$\bar{\omega}_{d,j}$		5.4536	21.5481	47.4007	60.0586	81.5000	121.6524
	$\bar{\omega}_{ud,j}$	17x17	5.4604	21.5748	47.6029	60.4627	82.4848	125.0324
	$\bar{\omega}_{d,j}$		5.4536	21.5479	47.3983	60.0586	81.4854	121.5917
	$\bar{\omega}_{ud,j}$	19x19	5.4604	21.5747	47.6016	60.4627	82.4768	124.9981
	$\bar{\omega}_{d,j}$		5.4536	21.5478	47.3971	60.0586	81.4777	121.5601

Table 2. The frequencies obtained for the P-S beam with different damping intensities

$\frac{L}{h}$	Study	ξ (%)	Mode 1	2	3	4	5	6
5	Full IGA	3						
	$\bar{\omega}_{ud,j}$		5.1552	15.1157	17.9110	34.3247	45.3470	52.3284
	$\bar{\omega}_{d,j}$		5.1529	15.1089	17.9013	34.2743	45.2369	52.1622
	Reduced IGA							
	$\bar{\omega}_{ud,j}$		5.1552	15.1157	17.9110	34.3247	45.3470	52.3284
	$\bar{\omega}_{d,j}$		5.1529	15.1089	17.9013	34.2743	45.2369	52.1622
	Full IGA	5						
	$\bar{\omega}_{ud,j}$		5.1552	15.1157	17.9110	34.3247	45.3470	52.3284
	$\bar{\omega}_{d,j}$		5.1488	15.0968	17.8840	34.1846	45.0404	51.8653
	Reduced IGA							
	$\bar{\omega}_{ud,j}$		5.1552	15.1157	17.9111	34.3363	45.3605	52.5144
	$\bar{\omega}_{d,j}$		5.1488	15.0968	17.8841	34.1981	45.0544	52.0658
	Full IGA	7						
	$\bar{\omega}_{ud,j}$		5.1552	15.1157	17.9110	34.3247	45.3470	52.3284
	$\bar{\omega}_{d,j}$		5.1426	15.0786	17.8580	34.0495	44.7441	51.4168
	Reduced IGA							
	$\bar{\omega}_{ud,j}$		5.1552	15.1006	17.9157	34.3111	45.5822	53.3105
	$\bar{\omega}_{d,j}$		5.1426	15.0650	17.8624	34.0080	44.9799	52.5203
20	Full IGA	3						
	$\bar{\omega}_{ud,j}$		5.4604	21.5748	47.6029	60.4627	82.4848	125.0324
	$\bar{\omega}_{d,j}$		5.4580	21.5651	47.5294	60.3176	82.1264	123.8048
	Reduced IGA							
	$\bar{\omega}_{ud,j}$		5.4604	21.5754	47.6342	60.4637	81.4421	123.5195
	$\bar{\omega}_{d,j}$		5.4580	21.5657	47.5659	60.3181	80.6858	122.3281
	Full IGA	5						
	$\bar{\omega}_{ud,j}$		5.4604	21.5748	47.6029	60.4627	82.4848	125.0324
	$\bar{\omega}_{d,j}$		5.4536	21.5479	47.3983	60.0586	81.4854	121.5917
	Reduced IGA							
	$\bar{\omega}_{ud,j}$		5.4604	21.5683	47.5513	60.4704	77.8388	107.9004
	$\bar{\omega}_{d,j}$		5.4536	21.5408	47.3539	60.0662	77.4884	107.8947

Table 2. (continued)

$\frac{L}{h}$	Study	ξ (%)	Mode 1	2	3	4	5	6
	Full IGA	7						
	$\bar{\omega}_{ud,j}$		5.4604	21.5748	47.6029	60.4627	82.4848	125.0324
	$\bar{\omega}_{d,j}$		5.4470	21.5219	47.2011	59.6681	80.5144	118.1943
	Reduced IGA							
	$\bar{\omega}_{ud,j}$		5.4604	21.5859	47.6234	60.5293	86.0098	127.6531
	$\bar{\omega}_{d,j}$		5.4470	21.5338	47.2328	59.7483	83.7990	121.2713

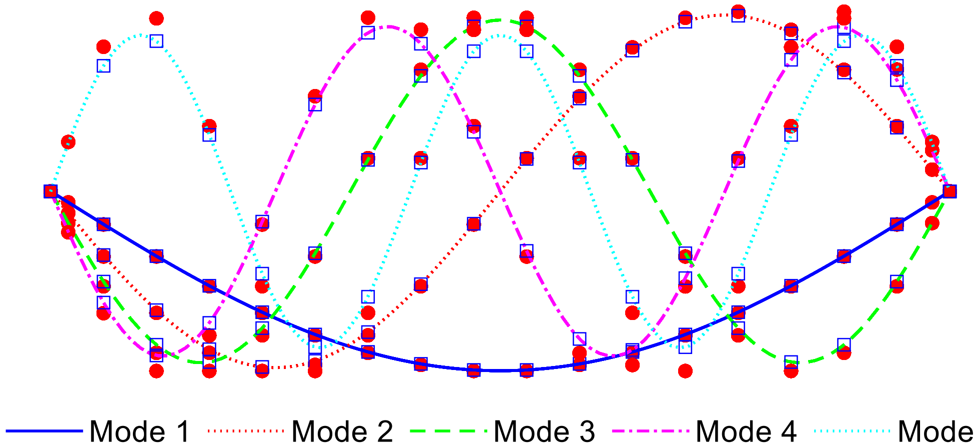

Fig. 3. The first five mode shapes of the P-S beam with the DOF w_0, $\frac{L}{h}=5$ and $\xi=5$ % given by the reduced-order IGA.

As a typical illustration, Fig. 3 displays the first five mode shapes with regard to the DOF w_0 attained by the reduced-order IGA and the full IGA with $\frac{L}{h}=5$ and $\xi=5\,\%$.

3.2. Clamped-free (C-F) beam

Herein, the C-F beam is investigated. According to this boundary condition, $u_0(0)=w_0(0)=\theta_0(0)=0$ are enforced. The same material properties as in the foregoing example are utilized. Table 3 shows the frequencies obtained by the present method for $\frac{L}{h}=5$ and $\frac{L}{h}=20$ with different intensities of the damping ratio involving $\xi=3\,\%$, $5\,\%$ and $7\,\%$. As expected, the undamped frequencies obtained by the reduced-order IGA are in good agreement with those of reference solutions without damping.

For demonstration, Fig. 4 plots the first five mode shapes of the C-F beam with the DOF w_0 given by the present method with $\frac{L}{h}=5$ and $\xi=5\,\%$.

3.3. Clamped-clamped (C-C) beam

In this example, the C-C beam, which is clamped at its two ends, is studied. For such a boundary condition, $u_0(0,L)=w_0(0,L)=\theta_0(0,L)=0$ are assigned. All material properties are kept as those of the foregoing examples. Comparisons of outcomes acquired by different methods are summarized in Table 4. It can be found that the reduced-order IGA can yield the undamped frequencies with high accuracy against other reference solutions. Moreover, the current method still calculates the damped frequencies with different damping amplitudes. Of course, the undamped frequencies are always larger than the damped ones.

Table 3. The frequencies obtained for the C-F beam with different damping intensities

$\frac{L}{h}$	Study	ξ (%)	Mode 1	2	3	4	5	6
5	$\bar{\omega}_{ud,j}$ [6]		-	-	-	-	-	-
	$\bar{\omega}_{ud,j}$ [7]		1.8957	-	-	-	-	-
	$\bar{\omega}_{ud,j}$ [8]		1.9055	-	-	-	-	-
	Full IGA	3						
	$\bar{\omega}_{ud,j}$		1.8961	10.2824	15.1157	24.6665	41.2635	45.3470
	$\bar{\omega}_{d,j}$		1.8953	10.2778	15.1033	24.6179	41.0448	45.0578
	Reduced IGA							
	$\bar{\omega}_{ud,j}$		1.8961	10.2832	15.1157	24.7058	41.5374	45.3683
	$\bar{\omega}_{d,j}$		1.8953	10.2785	15.1034	24.6547	41.3098	45.0799
	Full IGA	5						
	$\bar{\omega}_{ud,j}$		1.8961	10.2824	15.1157	24.6665	41.2635	45.3470
	$\bar{\omega}_{d,j}$		1.8937	10.2696	15.0814	24.5314	40.6532	44.5390
	Reduced IGA							
	$\bar{\omega}_{ud,j}$		1.8959	10.2139	15.1167	23.9903	40.1026	45.5329
	$\bar{\omega}_{d,j}$		1.8935	10.1939	15.0819	23.6529	38.7913	44.5583
	Full IGA	7						
	$\bar{\omega}_{ud,j}$		1.8961	10.2824	15.1157	24.6665	41.2635	45.3470
	$\bar{\omega}_{d,j}$		1.8915	10.2572	15.0483	24.4010	40.0586	43.7492
	Reduced IGA							
	$\bar{\omega}_{ud,j}$		1.8961	10.3423	15.1131	26.4004	44.6555	48.7368
	$\bar{\omega}_{d,j}$		1.8914	10.3045	15.0442	25.7313	42.7087	45.9446
20	$\bar{\omega}_{ud,j}$ [6]		-	-	-	-	-	-
	$\bar{\omega}_{ud,j}$ [7]		1.9496	-	-	-	-	-
	$\bar{\omega}_{ud,j}$ [8]		1.9527	-	-	-	-	-
	Full IGA	3						
	$\bar{\omega}_{ud,j}$		1.9496	12.0791	33.2291	60.4627	63.5473	102.0123
	$\bar{\omega}_{d,j}$		1.9487	12.0736	33.1415	59.9486	62.9508	99.5441
	Reduced IGA							
	$\bar{\omega}_{ud,j}$		1.9496	12.1135	35.0629	60.1352	76.4512	127.3800
	$\bar{\omega}_{d,j}$		1.9487	12.1037	34.7030	59.5534	72.8671	124.4853
	Full IGA	5						
	$\bar{\omega}_{ud,j}$		1.9496	12.0791	33.2291	60.4627	63.5473	102.0123
	$\bar{\omega}_{d,j}$		1.9472	12.0640	32.9851	59.0235	61.8763	94.9979
	Reduced IGA							
	$\bar{\omega}_{ud,j}$		1.9498	12.1466	34.4795	60.4009	71.0045	123.2478
	$\bar{\omega}_{d,j}$		1.9474	12.1325	34.3105	58.9264	70.0715	112.2505
	Full IGA	7						
	$\bar{\omega}_{ud,j}$		1.9496	12.0791	33.2291	60.4627	63.5473	102.0123
	$\bar{\omega}_{d,j}$		1.9448	12.0495	32.7492	57.6081	60.2286	87.7381

Table 3. (continued)

$\frac{L}{h}$	Study	ξ (%)	Mode 1	2	3	4	5	6
	Reduced IGA							
	$\overline{\omega}_{ud,j}$		1.9496	12.0824	33.3987	60.2718	63.7372	108.8485
	$\overline{\omega}_{d,j}$		1.9448	12.0524	32.8712	57.4403	59.8438	94.1749

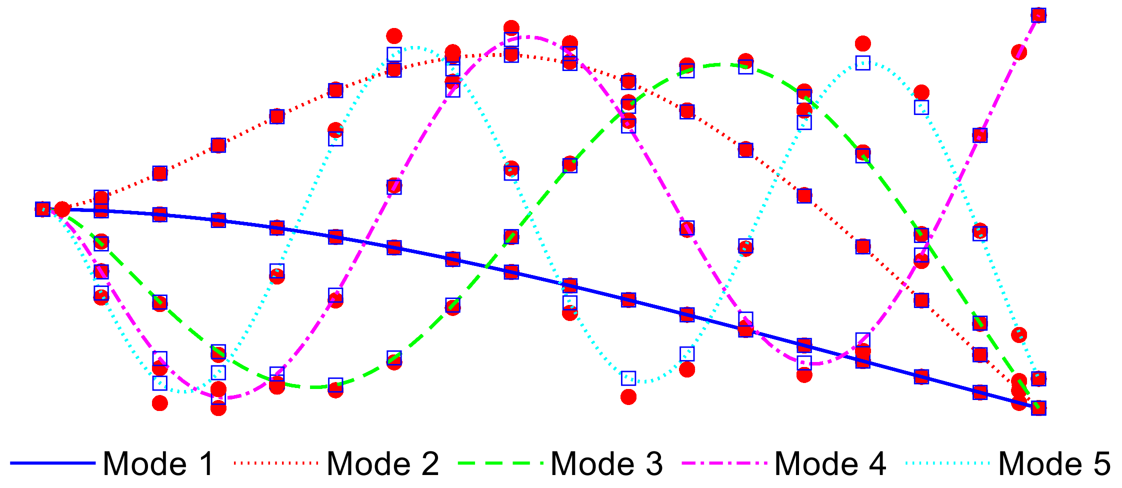

Fig. 4. The first five mode shapes of the C-F beam with the DOF w_0, $\frac{L}{h}=5$ and $\xi=5$ % given by the reduced-order IGA

Table 4. The frequencies obtained for the C-C beam with different damping intensities

$\frac{L}{h}$	Study	ξ (%)	Mode 1	2	3	4	5	6
5	$\overline{\omega}_{ud,j}$ [6]		-	-	-	-	-	-
	$\overline{\omega}_{ud,j}$ [7]		10.0726	-	-	-	-	-
	$\overline{\omega}_{ud,j}$ [8]		10.1851	-	-	-	-	-
	Full IGA	3						
	$\overline{\omega}_{ud,j}$		10.1260	23.5061	30.2314	39.6365	57.2040	60.4627
	$\overline{\omega}_{d,j}$		10.1214	23.4955	30.2139	39.6036	57.1182	60.3629
	Reduced IGA							
	$\overline{\omega}_{ud,j}$		10.1260	23.5061	30.2314	39.6365	57.2040	60.4627
	$\overline{\omega}_{d,j}$		10.1214	23.4955	30.2139	39.6036	57.1182	60.3629
	Full IGA	5						
	$\overline{\omega}_{ud,j}$		10.1260	23.5061	30.2314	39.6365	57.2040	60.4627
	$\overline{\omega}_{d,j}$		10.1133	23.4767	30.1828	39.5451	56.9654	60.1850
	Reduced IGA							
	$\overline{\omega}_{ud,j}$		10.1260	23.5061	30.2314	39.6365	57.2040	60.4627
	$\overline{\omega}_{d,j}$		10.1133	23.4767	30.1828	39.5451	56.9654	60.1850
	Full IGA	7						
	$\overline{\omega}_{ud,j}$		10.1260	23.5061	30.2314	39.6365	57.2040	60.4627
	$\overline{\omega}_{d,j}$		10.1011	23.4485	30.1361	39.4572	56.7355	59.9171

Table 4. (continued)

$\frac{L}{h}$	Study	ξ (%)	Mode 1	2	3	4	5	6
	Reduced IGA							
	$\overline{\omega}_{ud,j}$		10.1260	23.5061	30.2314	39.6365	57.2040	60.4627
	$\overline{\omega}_{d,j}$		10.1011	23.4485	30.1361	39.4572	56.7355	59.9171
20	$\overline{\omega}_{ud,j}$ [6]		-	-	-	-	-	-
	$\overline{\omega}_{ud,j}$ [7]		12.2243	-	-	-	-	-
	$\overline{\omega}_{ud,j}$ [8]		12.2660	-	-	-	-	-
	Full IGA	3						
	$\overline{\omega}_{ud,j}$		12.2270	33.0209	63.0808	101.1440	120.9255	146.0827
	$\overline{\omega}_{d,j}$		12.2215	33.0061	63.0139	100.8979	120.5143	145.3696
	Reduced IGA							
	$\overline{\omega}_{ud,j}$		12.2270	33.0207	63.0117	99.7787	120.9250	155.2528
	$\overline{\omega}_{d,j}$		12.2215	33.0057	62.9329	99.7160	120.5127	153.9082
	Full IGA	5						
	$\overline{\omega}_{ud,j}$		12.2270	33.0209	63.0808	101.1440	120.9255	146.0827
	$\overline{\omega}_{d,j}$		12.2117	32.9796	62.8946	100.4591	119.7800	144.0932
	Reduced IGA							
	$\overline{\omega}_{ud,j}$		12.2270	33.0229	63.2597	98.4143	120.8861	153.6706
	$\overline{\omega}_{d,j}$		12.2117	32.9817	63.1124	97.5556	119.7327	152.9365
	Full IGA	7						
	$\overline{\omega}_{ud,j}$		12.2270	33.0209	63.0808	101.1440	120.9255	146.0827
	$\overline{\omega}_{d,j}$		12.1970	32.9399	62.7153	99.7971	118.6699	142.1570
	Reduced IGA							
	$\overline{\omega}_{ud,j}$		12.2270	33.0254	63.6512	104.3782	120.8384	170.0926
	$\overline{\omega}_{d,j}$		12.1970	32.9442	63.3322	102.9278	118.5642	147.3311

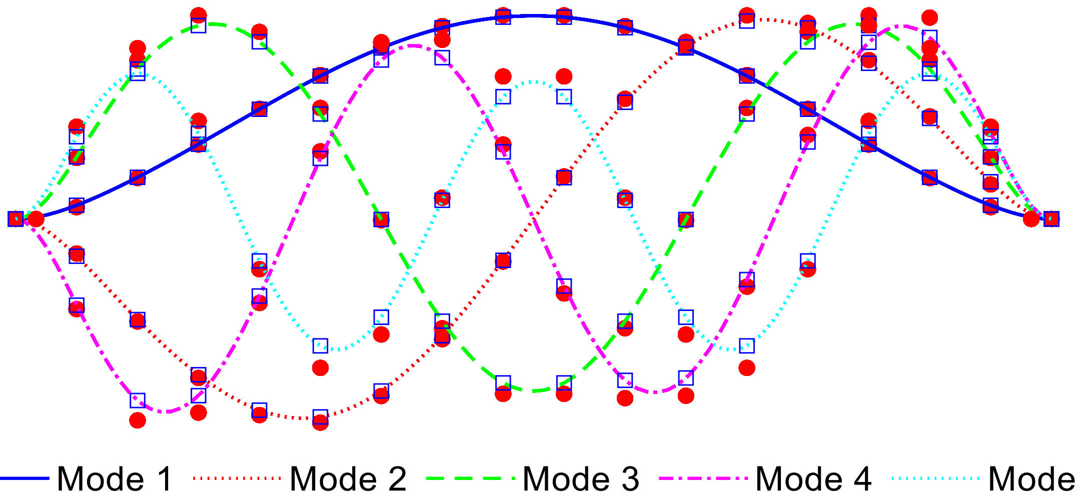

Fig. 5. The first five mode shapes of the C-C beam with the DOF w_0, $\frac{L}{h} = 5$ and $\xi = 5$ % given by the reduced-order IGA

Analogously, the first five mode shapes of the C-C beam with the DOF w_0, $\frac{L}{h}=5$ and $\xi=5\,\%$ attained by the present method are displayed in Fig. 5.

3.4. Clamped-pinned (C-P) beam

As the last example illustrated in this work, a clamped-pinned beam is studied. With these boundary conditions, $u_0(0)=w_0(0)=\theta_0(0)=0$ and $u_0(L)=w_0(L)=0$ are applied. This example holds all material parameters defined in the foregoing examples.

Table 5 reports the undamped and damped frequencies obtained from the reduced-order IGA. It can be recognized that the undamped frequencies match well with those of reference solutions. Meanwhile, the damped frequencies are always smaller than the undamped ones. The larger the discrepancy between these two values is, the higher the modal mode order is. This proves that the damping effect on the vibration behavior of the beam is crucial. If this factor is omitted in vibration analysis, the obtained results can incorrectly reflect the real behavior of a structure.

Ultimately, the first five mode shapes of the C-P beam with the DOF w_0, $\frac{L}{h}=5$ and $\xi=5\,\%$ gained by the reduced-order IGA are plotted in Fig. 6.

Table 5. The frequencies obtained for the C-P beam with different damping intensities

$\frac{L}{h}$	Study	ξ (%)	Mode					
			1	2	3	4	5	6
5	$\bar{\omega}_{ud,j}$ [6]		-	-	-	-	-	-
	$\bar{\omega}_{ud,j}$ [7]		-	-	-	-	-	-
	$\bar{\omega}_{ud,j}$ [8]		-	-	-	-	-	-
	Full IGA	3						
	$\bar{\omega}_{ud,j}$		7.5085	20.7768	30.2314	37.0273	54.8007	60.4627
	$\bar{\omega}_{d,j}$		7.5051	20.7674	30.2101	36.9918	54.6982	60.3274
	Reduced IGA							
	$\bar{\omega}_{ud,j}$		7.5085	20.7768	30.2314	37.0273	54.8007	60.4627
	$\bar{\omega}_{d,j}$		7.5051	20.7674	30.2101	36.9918	54.6982	60.3274
	Full IGA	5						
	$\bar{\omega}_{ud,j}$		7.5085	20.7768	30.2314	37.0273	54.8007	60.4627
	$\bar{\omega}_{d,j}$		7.4991	20.7508	30.1721	36.9287	54.5155	60.0861
	Reduced IGA							
	$\bar{\omega}_{ud,j}$		7.5085	20.7768	30.2314	37.0273	54.8007	60.4627
	$\bar{\omega}_{d,j}$		7.4991	20.7508	30.1721	36.9287	54.5155	60.0861
	Full IGA	7						
	$\bar{\omega}_{ud,j}$		7.5085	20.7768	30.2314	37.0273	54.8007	60.4627
	$\bar{\omega}_{d,j}$		7.4901	20.7258	30.1152	36.8339	54.2402	59.7223
	Reduced IGA							
	$\bar{\omega}_{ud,j}$		7.5085	20.7772	30.2314	37.0512	55.0238	60.4632
	$\bar{\omega}_{d,j}$		7.4901	20.7263	30.1152	36.8600	54.4819	59.7229
20	$\bar{\omega}_{ud,j}$ [6]		-	-	-	-	-	-
	$\bar{\omega}_{ud,j}$ [7]		-	-	-	-	-	-

Table 5. (continued)

$\frac{L}{h}$	Study	ξ (%)	Mode 1	2	3	4	5	6
	$\bar{\omega}_{ud,j}$ [8]		-	-	-	-	-	-
	Full IGA	3						
	$\bar{\omega}_{ud,j}$		8.4832	27.0461	55.1517	91.6883	120.9255	135.4844
	$\bar{\omega}_{d,j}$		8.4794	27.0339	55.0825	91.3979	120.2734	134.5725
	Reduced IGA							
	$\bar{\omega}_{ud,j}$		8.4832	27.0478	55.2169	89.9448	120.8899	144.5308
	$\bar{\omega}_{d,j}$		8.4794	27.0355	55.1389	89.2350	120.2416	144.4677
	Full IGA	5						
	$\bar{\omega}_{ud,j}$		8.4832	27.0461	55.1517	91.6883	120.9255	135.4844
	$\bar{\omega}_{d,j}$		8.4726	27.0122	54.9593	90.8792	119.1054	132.9358
	Reduced IGA							
	$\bar{\omega}_{ud,j}$		8.4832	27.0479	55.1896	94.4434	120.8413	146.6337
	$\bar{\omega}_{d,j}$		8.4726	27.0137	54.9773	93.3136	118.9997	-
	Full IGA	7						
	$\bar{\omega}_{ud,j}$		8.4832	27.0461	55.1517	91.6883	120.9255	135.4844
	$\bar{\omega}_{d,j}$		8.4624	26.9797	54.7739	90.0957	117.3315	130.4424
	Reduced IGA							
	$\bar{\omega}_{ud,j}$		8.4833	27.0729	55.5458	99.0035	120.5696	164.2337
	$\bar{\omega}_{d,j}$		8.4624	27.0061	55.1648	97.2084	116.9223	149.9452

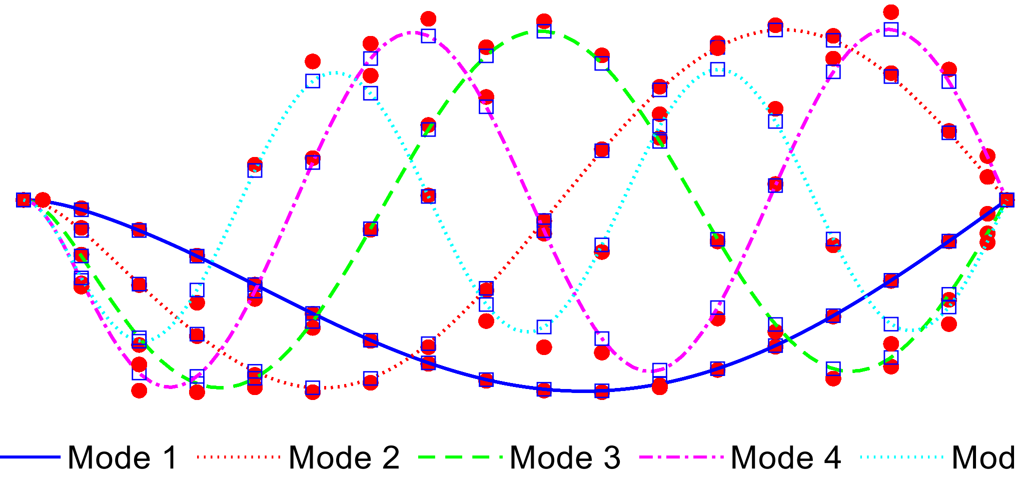

Fig. 6. The first five mode shapes of the C-P beam with the DOF w_0, $\frac{L}{h}=5$ and $\xi=5$ % given by the reduced-order IGA

3.5. Validation and discussion on the accuracy of the proposed model

The validation of the proposed formulation is summarized in Table 6 for $\xi=3$ % as a typical case. In this study, the validation is conducted at three levels. First, the full IGA model based on the fifth-order GSDT is verified in the damping-free limit by comparison with the existing references [6, 7, 8] reported in the literature. This comparison is appropriate because the existing benchmark studies mainly provide undamped natural frequencies. As shown in Table 6, the present full

IGA results agree well with the reference solutions for different boundary conditions and span-to-height ratios, especially for the P-S, C-F and C-C beams.

After the full-order model is verified, the reduced-order IGA model is assessed by comparison with the corresponding full IGA solutions. The results show that the reduced model can accurately reproduce the lower-order frequencies of the full model, which are the most relevant in practical vibration analysis. Some larger discrepancies may appear in higher modes because only selected master DOFs are retained in the reduced formulation. Therefore, the accuracy of the reduced model depends on the selected master DOFs and the modal range of interest.

For the damped cases, no directly comparable benchmark solutions are available for the same fifth-order GSDT–IGA–ROM framework. Therefore, the damping results are validated through their consistency with the full IGA model and the expected physical behavior of damped systems. In all investigated cases, the damped frequencies are lower than the corresponding undamped frequencies, and the reduction becomes more evident when the damping ratio increases. This confirms that the proposed reduced-order IGA model is both numerically consistent and physically reasonable for damped vibration analysis of beams.

Table 6. Validation of the proposed formulation for the beam under different boundary conditions with $\xi = 3$ %

Boundary conditions	$\frac{L}{h}$	Study	Mode 1	Mode 2	Mode 3	Mode 4	Mode 5	Mode 6
P-S	5	$\bar{\omega}_{ud,j}$ [6]	5.1527	17.8812	34.2097	-	-	-
		$\bar{\omega}_{ud,j}$ [7]	5.1528	17.8817	34.2143	-	-	-
		$\bar{\omega}_{ud,j}$ [8]	5.1618	-	-	-	-	-
		Full IGA						
		$\bar{\omega}_{ud,j}$	5.1552	15.1157	17.9110	34.3247	45.3470	52.3284
		$\bar{\omega}_{d,j}$	5.1529	15.1089	17.9013	34.2743	45.2369	52.1622
		Reduced IGA						
		$\bar{\omega}_{ud,j}$	5.1552	15.1157	17.9110	34.3247	45.3470	52.3284
		$\bar{\omega}_{d,j}$	5.1529	15.1089	17.9013	34.2743	45.2369	52.1622
		$\bar{\omega}_{ud,j}$ [6]	5.4603	21.5732	47.5930	-	-	-
		$\bar{\omega}_{ud,j}$ [7]	5.4603	21.5732	47.5999	-	-	-
		$\bar{\omega}_{ud,j}$ [8]	5.4610	-	-	-	-	-
	20	Full IGA						
		$\bar{\omega}_{ud,j}$	5.4604	21.5748	47.6029	60.4627	82.4848	125.0324
		$\bar{\omega}_{d,j}$	5.4580	21.5651	47.5294	60.3176	82.1264	123.8048
		Reduced IGA						
		$\bar{\omega}_{ud,j}$	5.4604	21.5754	47.6342	60.4637	81.4421	123.5195
		$\bar{\omega}_{d,j}$	5.4580	21.5657	47.5659	60.3181	80.6858	122.3281
C-F	5	$\bar{\omega}_{ud,j}$ [6]	-	-	-	-	-	-
		$\bar{\omega}_{ud,j}$ [7]	1.8957	-	-	-	-	-
		$\bar{\omega}_{ud,j}$ [8]	1.9055	-	-	-	-	-
		Full IGA						
		$\bar{\omega}_{ud,j}$	1.8961	10.2824	15.1157	24.6665	41.2635	45.3470

Table 6. (continued)

Boundary conditions	$\frac{L}{h}$	Study	Mode 1	2	3	4	5	6
		$\bar{\omega}_{d,j}$	1.8953	10.2778	15.1033	24.6179	41.0448	45.0578
		Reduced IGA						
		$\bar{\omega}_{ud,j}$	1.8961	10.2832	15.1157	24.7058	41.5374	45.3683
		$\bar{\omega}_{d,j}$	1.8953	10.2785	15.1034	24.6547	41.3098	45.0799
	20	$\bar{\omega}_{ud,j}$ [6]	-	-	-	-	-	-
		$\bar{\omega}_{ud,j}$ [7]	1.9496	-	-	-	-	-
		$\bar{\omega}_{ud,j}$ [8]	1.9527	-	-	-	-	-
		Full IGA						
		$\bar{\omega}_{ud,j}$	1.9496	12.0791	33.2291	60.4627	63.5473	102.0123
		$\bar{\omega}_{d,j}$	1.9487	12.0736	33.1415	59.9486	62.9508	99.5441
		Reduced IGA						
		$\bar{\omega}_{ud,j}$	1.9496	12.1135	35.0629	60.1352	76.4512	127.3800
		$\bar{\omega}_{d,j}$	1.9487	12.1037	34.7030	59.5534	72.8671	124.4853
C-C	5	$\bar{\omega}_{ud,j}$ [6]	-	-	-	-	-	-
		$\bar{\omega}_{ud,j}$ [7]	10.0726	-	-	-	-	-
		$\bar{\omega}_{ud,j}$ [8]	10.1851	-	-	-	-	-
		Full IGA						
		$\bar{\omega}_{ud,j}$	10.1260	23.5061	30.2314	39.6365	57.2040	60.4627
		$\bar{\omega}_{d,j}$	10.1214	23.4955	30.2139	39.6036	57.1182	60.3629
		Reduced IGA						
		$\bar{\omega}_{ud,j}$	10.1260	23.5061	30.2314	39.6365	57.2040	60.4627
		$\bar{\omega}_{d,j}$	10.1214	23.4955	30.2139	39.6036	57.1182	60.3629
	20	$\bar{\omega}_{ud,j}$ [6]	-	-	-	-	-	-
		$\bar{\omega}_{ud,j}$ [7]	12.2243	-	-	-	-	-
		$\bar{\omega}_{ud,j}$ [8]	12.2660	-	-	-	-	-
		Full IGA						
		$\bar{\omega}_{ud,j}$	12.2270	33.0209	63.0808	101.1440	120.9255	146.0827
		$\bar{\omega}_{d,j}$	12.2215	33.0061	63.0139	100.8979	120.5143	145.3696
		Reduced IGA						
		$\bar{\omega}_{ud,j}$	12.2270	33.0207	63.0117	99.7787	120.9250	155.2528
		$\bar{\omega}_{d,j}$	12.2215	33.0057	62.9329	99.7160	120.5127	153.9082

4. Conclusions

The vibration behavior of beams with the damping effect was analyzed in this work using the reduced-order IGA in state space. In which, the fifth-order polynomial functions and B-spline functions are used to represent the displacements across the height and the length of a beam, respectively. The IGA condensed in state space with only a given number of DOFs in place of all ones is employed for analyzing vibration responses with damping. The influences of different boundaries, span-to-height ratios and damping magnitudes on the damped vibration of a beam are studied. Several conclusions can be drawn as follows:

There are zero transverse shear stresses at the top and bottom surfaces of the beam with the fifth-order GSDT. In addition, no any shear correction coefficients are required.

High-order derivatives in the formulas derived from the fifth-order GSDT can be simply satisfied by the prominent properties of B-spline basis functions within the IGA.

Undamped frequencies, which are inferred from damped ones, obtained by the reduced-order IGA agree well with those of other existing articles. This confirms the accuracy and reliability of the current method.

Damped frequencies are always smaller than undamped ones for the same mode. This is caused by the damping effect. The larger the discrepancy becomes, the higher the damping ratio is, especially for high-order modes.

Vibration responses with and without damping are significantly affected by different boundary conditions and span-to-height ratios, especially for damping intensities. Higher damping values will be studied soon.

Acknowledgments

This research is funded by Vietnam National Foundation for Science and Technology Development (NAFOSTED) under grant number 107.02-2025.13.

Declaration of Generative AI

During the preparation of this work, the authors do not use Generative AI and AI-assisted technologies tools in order to generate the content of the manuscript.

References

[1] O.A. Bauchau, J.I. Craig. (2009). Euler-Bernoulli beam theory. *Structural Analysis. Springer, pp. 173–221.* https://doi.org/10.1007/978-90-481-2516-6_5

[2] A. Öchsner. (2021). Timoshenko Beam Theory. *Classical Beam Theories of Structural Mechanics, Springer, pp. 67–104.* https://doi.org/10.1007/978-3-030-76035-9_3

[3] X.-F. Li, B.-L. Wang, J.-C. Han. (2010). A higher-order theory for static and dynamic analyses of functionally graded beams. *Archive of Applied Mechanics*, 80, 1197–1212. https://doi.org/10.1007/s00419-010-0435-6

[4] R. Kadoli, K. Akhtar, N. Ganesan. (2008). Static analysis of functionally graded beams using higher order shear deformation theory. *Applied Mathematical Modelling*, 32(12), 2509–2525. https://doi.org/10.1016/j.apm.2007.09.015

[5] M. Karama, K.S. Afaq, S. Mistou. (2003). Mechanical behaviour of laminated composite beam by the new multi-layered laminated composite structures model with transverse shear stress continuity. *International Journal of Solids and Structures*, 40(6), 1525–1546. https://doi.org/10.1016/S0020-7683(02)00647-9

[6] H.-T. Thai, T.P. Vo. (2012). Bending and free vibration of functionally graded beams using various higher-order shear deformation beam theories. *International Journal of Mechanical Sciences*, 62(1), 57–66. https://doi.org/10.1016/j.ijmecsci.2012.05.014

[7] T.-K. Nguyen, T.T.-P. Nguyen, T.P. Vo, H.-T. Thai. (2015). Vibration and buckling analysis of functionally graded sandwich beams by a new higher-order shear deformation theory. *Composites Part B: Engineering*, 76, 273–285. https://doi.org/10.1016/j.compositesb.2015.02.032

[8] T.P. Vo, H.-T. Thai, T.-K. Nguyen, F. Inam, J. Lee. (2015). A quasi-3D theory for vibration and buckling of functionally graded sandwich beams. *Composite Structures*, 119, 1–12. https://doi.org/10.1016/j.compstruct.2014.08.006

[9] G. Prathap, G.R. Bhashyam. (1982). Reduced integration and the shear-flexible beam element. *International Journal for Numerical Methods in Engineering*, 18(2), 195–210. https://doi.org/10.1002/nme.1620180205

[10] J. Choit, J. Lim. (1995). General curved beam elements based on the assumed strain fields.

Computers & Structures, 55(3), 379–386. https://doi.org/10.1016/0045-7949(95)98865-N

[11] A. Patton, L. Leonetti, J. Kiendl. (2025). An isogeometric assumed natural strain method to alleviate locking in solid beams. *Computer Methods in Applied Mechanics and Engineering*, 442, 118024. https://doi.org/10.1016/j.cma.2025.118024

[12] T.J.R. Hughes, J.A. Cottrell, Y. Bazilevs. (2005). Isogeometric analysis: CAD, finite elements, NURBS, exact geometry and mesh refinement. *Computer Methods in Applied Mechanics and Engineering*, 194(39-41), 4135–4195. https://doi.org/10.1016/j.cma.2004.10.008

[13] J. Kiendl, Y. Bazilevs, M.-C. Hsu, R. Wüchner, K.-U. Bletzinger. (2010). The bending strip method for isogeometric analysis of Kirchhoff–Love shell structures comprised of multiple patches. *Computer Methods in Applied Mechanics and Engineering*, 199(37-40), 2403–2416. https://doi.org/10.1016/j.cma.2010.03.029

[14] Q.X. Lieu, J. Lee. (2017). A multi-resolution approach for multi-material topology optimization based on isogeometric analysis. *Computer Methods in Applied Mechanics and Engineering*, 323, 272–302. https://doi.org/10.1016/j.cma.2017.05.009

[15] Q.X. Lieu, J. Lee. (2019). An isogeometric multimesh design approach for size and shape optimization of multidirectional functionally graded plates. *Computer Methods in Applied Mechanics and Engineering*, 343, 407–437. https://doi.org/10.1016/j.cma.2018.08.017

[16] Q.X. Lieu. (2024). An optimization-assisted reduced order model for dynamics of plates using isogeometric analysis. *Thin-Walled Structures*, 202, 112078. https://doi.org/10.1016/j.tws.2024.112078

[17] H.R. Atri, S. Shojaee. (2016). Free Vibration Analysis of Thin-Shell Structures Using Finite Element Based on Isogeometric Approach. *Iranian Journal of Science and Technology, Transactions of Civil Engineering*, 40, 85–96. https://doi.org/10.1007/s40996-016-0011-6

[18] N. Nguyen-Thanh, W. Li, K. Zhou. (2018). Static and free-vibration analyses of cracks in thin-shell structures based on an isogeometric-meshfree coupling approach. *Computational Mechanics*, 62, 1287–1309. https://doi.org/10.1007/s00466-018-1564-y

[19] K.A. Hasim, A. Kefal. (2025). Free and forced vibration analysis of piezolaminated plates via an isogeometric layerwise finite element. *Mechanics of Advanced Materials and Structures*, 32(17), 4146–4161. https://doi.org/10.1080/15376494.2024.2400716

[20] K.D. Dang, N.H. Nguyen, S. Lee, V.H. Luong, T.A. Le, Q.X. Lieu. (2023). A novel model order reduction-based two-stage damage detection paradigm for trusses using time–history acceleration. *Advances in Engineering Software*, 176, 103374. https://doi.org/10.1016/j.advengsoft.2022.103374

[21] Q.X. Lieu. (2023). A novel multistage damage detection method for trusses using time-history data based on model order reduction and deep neural network. *Mechanical Systems and Signal Processing*, 200, 110635. https://doi.org/10.1016/j.ymssp.2023.110635

[22] Z.-Q. Qu. (2004). Model Order Reduction Techniques with Applications in Finite Element Analysis. *Springer*. https://doi.org/10.1007/978-1-4471-3827-3

[23] N.-T. Nguyen, D. Hui, J. Lee, H. Nguyen-Xuan. (2015). An efficient computational approach for size-dependent analysis of functionally graded nanoplates. *Computer Methods in Applied Mechanics and Engineering*, 297, 191–218. https://doi.org/10.1016/j.cma.2015.07.021

[24] V.H. Luong, K.D. Dang, S. Lee, Q.X. Lieu.

(2025). Optimization of model order reduction for transient analysis of functionally graded plates using isogeometric analysis based on four-variable quasi-3D theory. *Composite Structures*, 355, 118844. https://doi.org/10.1016/j.compstruct.2025.118844

[25] Q.X. Lieu, Q.M. Lieu, T.T. Nguyen. (2026). Reduced-order isogeometric model in state space for damped vibration and dynamic analyses of functionally graded plates supported by Visco-Winkler–Pasternak foundation. *Composite Structures*, 377, 119877. https://doi.org/10.1016/j.compstruct.2025.119877

[26] C. de Boor. (1972). On calculating with B-splines. *Journal of Approximation Theory*, 6(1), 50–62. https://doi.org/10.1016/0021-9045(72)90080-9

[27] R.W. Clough. (2015). Dynamics of Structures. Second Edition. *CBS Publishers & Distributors.*

[28] Z.-Q. Qu, R.P. Selvam, Y. Jung. (2003). Model condensation for non-classically damped systems-Part II: Iterative schemes for dynamic condensation. *Mechanical Systems and Signal Processing*, 17(5), 1017–1032. https://doi.org/10.1006/mssp.2002.1527

[29] J.N. Reddy. (1984). A Simple Higher-Order Theory for Laminated Composite Plates. *Journal of Applied Mechanics*, 51(4), 745-752. https://doi.org/10.1115/1.3167719